frontiers | Frontiers in Remote Sensing

TYPE Original Research
PUBLISHED 02 July 2025
DOI 10.3389/frsen.2025.1606549

OPEN ACCESS

EDITED BY
Zenghui Zhang,
Shanghai Jiao Tong University, China

REVIEWED BY
Nuno Mouta,
Centro de Investigacao em Biodiversidade e Recursos Geneticos (CIBIO-InBIO), Portugal
Ebrahim Ghaderpour,
Sapienza University of Rome, Italy

*CORRESPONDENCE
Danling Tang,
lingzistdl@126.com
Hong Du,
hdu@stu.edu.cn

RECEIVED 05 April 2025
ACCEPTED 09 June 2025
PUBLISHED 02 July 2025

CITATION
Chen Q, Shen C, Du H and Tang D (2025) Comparing supervised classification algorithm–feature combinations for *Spartina alterniflora* extraction: a case study in Zhanjiang, China.
Front. Remote Sens. 6:1606549.
doi: 10.3389/frsen.2025.1606549

Comparing supervised classification algorithm–feature combinations for *Spartina alterniflora* extraction: a case study in Zhanjiang, China

Qiujie Chen[1,2], Chunyan Shen[3], Hong Du[2]* and Danling Tang[1]*

[1]Guangdong Remote Sensing Center for Marine Ecology and Environment, Southern Marine Science and Engineering Guangdong Laboratory (Guangzhou), Guangzhou, China, [2]Guangdong Provincial Key Laboratory of Marine Disaster Prediction and Prevention, Shantou University, Shantou, China, [3]College of Fisheries, Guangdong Ocean University, Zhanjiang, China

Mangrove forests are vital blue carbon ecosystems whose security is increasingly threatened by the non-native species *Spartina alterniflora*. Accurate remote sensing-based identification and monitoring are crucial for invasive species management; however, such methods have rarely been applied to determine the distribution of *S. alterniflora* in Zhanjiang, China. Here, we combined five supervised classification algorithms—random forest (RF), support vector machine, maximum likelihood classification (MLC), minimum distance classification, and Mahalanobis distance classification—with spectral bands, spectral indices, and the gray-level co-occurrence matrix (GLCM) derived from Sentinel-2 imagery to identify the optimal combination for monitoring the spatial distribution of *S. alterniflora* on Donghai Island, Zhanjiang. The sample dataset was divided into training and validation sets at a ratio of 7:3, yielding a sub-dataset with Jeffries–Matusita distances of 1.893–2.000, which satisfied classification requirements. The most accurate algorithm–feature combination was MLC plus spectral features, which achieved a kappa coefficient of 0.9061, an overall accuracy of 95.32%, and a similar extracted area (72.51 ha) to that derived from visual interpretation (68.7 ha). The next most accurate combinations were RF plus spectral bands + GLCM and RF plus spectral bands + spectral indices + GLCM, with kappa coefficients of 0.8991, overall accuracy of 94.96%, and extraction areas of 74.76 ha and 75.31 ha, respectively. RF showed superior adaptability across different feature scenarios, resulting in stable accuracy and minimal area error. According to visual interpretation, the area of *S. alterniflora* increased by 3.35 ha over a 5-year period, indicating a growth rate of 5.13%. By evaluating the accuracy of different classification methods and features, this research can facilitate *S. alterniflora* extraction and provide support for mangrove conservation efforts.

KEYWORDS

random forest (RF), maximum likelihood classification (MLC), sentinel-2, Spartina alterniflora, machine learning

1 Introduction

Mangrove forests represent a major blue carbon coastal ecosystem that plays a significant role in carbon sequestration and storage (Ahmed et al., 2017; Sidik et al., 2023). However, non-native species pose a substantial threat to mangrove habitats by encroaching on the survival space of native vegetation and disrupting local ecosystems and biodiversity (Dawson et al., 2017). In 1979, China introduced *Spartina alterniflora* (also known as *Sporobolus alterniflorus*) as an ecologically engineered species, primarily for its functions in shoreline stabilization and wind protection (Chung, 2006). *S. alterniflora* has also been introduced to West Coast of North America, Europe, and New Zealand, where it exhibits remarkable adaptability to various environmental conditions, achieving rapid habitat expansion through both sexual and asexual reproduction (Ainouche et al., 2004; Morris et al., 2005; Hartley et al., 2020). Owing to its continued encroachment on the habitats of native species, *S. alterniflora* has established itself as the dominant plant in local salt marshes (Zhu et al., 2016; Banerjee et al., 2022). In 2022, China formulated a special action plan aimed at controlling *S. alterniflora*, which aspired to eliminate ecological hazards in coastal wetlands by 2025 and curtail the unrestricted spread of this invasive species (National Forestry and Grassland Administration, 2025). Zhanjiang City, which houses the largest natural mangrove reserves in China, has been significantly affected by *S. alterniflora* invasion, resulting in extensive clean-up efforts. Effective monitoring of *S. alterniflora* is essential for identifying its distribution and dispersal mechanisms, thereby enabling the implementation of more effective removal strategies.

Traditional estimates of *S. alterniflora* extent rely on extensive field surveys, which can be costly and inadequate for capturing the overall distribution. In contrast, satellite remote sensing offers an effective means of terrestrial observation by providing a wealth of imagery for vegetation monitoring. Over the past 2 decades, multi-source remote sensing imagery and spectral indices have been frequently utilized for the long-term monitoring of *S. alterniflora*. Spectral indices are derived through band math to highlight the characteristic information of the target and reduce noise interference. They have applications in agricultural monitoring, water body extraction, etc., (Du et al., 2016; Li M et al., 2022). In the application of *S. alterniflora*, Xu et al. (2018) extracted long-term area data from Landsat TM and ETM + images of Changxing and Hengsha Islands from 1987 to 2016; O'Donnell and Schalles (2016) used Landsat 5 TM imagery and indices such as the normalized difference vegetation index (NDVI) and modified soil adjusted vegetation index (mSAVI) to extract 28 years of aboveground biomass data for *S. alterniflora* along the Central Georgia Coast; and Zhao et al. (2009) combined NDVI, mSAVI, enhanced vegetation index (EVI), and moderate-resolution imaging spectroradiometer imagery to analyze the spatiotemporal dynamic trends of *S. alterniflora* on Chongming Dongtan from 2001 to 2006.

The Sentinel-2 image has a resolution of 10 m and has achieved good classification application results in various fields. It can be used for land cover classification and forest health monitoring, and has also achieved remarkable results in disasters such as floods and avalanches (Candotti et al., 2022; Chu et al., 2024; Sharma et al., 2024; Aryal et al., 2025). To obtain more accurate information on *S. alterniflora*, Sentinel-2 is highly favored. Tian et al. (2020) used it to extract the expansion rate of *S. alterniflora*; Min et al. (2023) used Sentinel-2 to map the time and location of *S. alterniflora* removal work. In terms of classification algorithms, maximum likelihood classification (MLC) belongs to the statistical method category and is applied in mineral identification (Ondieki, 2022); support vector machine (SVM) and random forest (RF) belong to machine learning algorithms, which improve classification accuracy by adjusting optimal parameters and are applied in urban land classification and tree species classification (Hanif et al., 2023; Saim and Aly, 2025). In the case of *S. alterniflora*, Ai et al. (2017) utilized GF-1 WFV data based on phenological characteristics and extracted time-series information on *S. alterniflora* in the Yangtze River Estuary using SVM and MLC methods. Zhang et al. (2021) applied RF algorithms to key features from Sentinel-1 and Sentinel-2 imagery to extract area data from the Yellow River Delta. Additionally, advance in deep learning technology have led to the increasing application of algorithms such as U-Net, convolutional neural networks, and extreme gradient boosting to *S. alterniflora* extraction (Fu et al., 2022; Li Y et al., 2022b; Zhu et al., 2022). Furthermore, currently the most popular one is Google Earth Engine (GEE), which integrates mainstream classification algorithms and has Sentinel-2 and Landsat series data that can be filtered and called online (Min et al., 2023; Hosseini et al., 2024). It has also been applied in fields such as agriculture and *S. alterniflora* extraction (Zhou et al., 2024).

Compared to other regions, Zhanjiang has relatively limited and incomplete statistical data on the distribution of *S. alterniflora*. Liu et al. (2018) noted the presence of *S. alterniflora* patches in Zhanjiang during nationwide data extraction, and further field surveys revealed that the extent of *S. alterniflora* in the mangrove protection area reached 12.59 ha and encompassed five counties and districts within the city (Xin et al., 2018). Subsequently, Huang et al. (2021) employed object-based classification techniques to extract the area of *S. alterniflora* for 2016–2018, which indicated a substantial increase to 157.05 ha, highlighting the severe scale of *S. alterniflora* invasion in this region. However, remote sensing-based evaluations of *S. alterniflora* in Zhanjiang remain relatively scarce, and no studies have determined the most suitable classification methods and features for this region.

Therefore, in this study, we employ Sentinel-2 imagery to extract *S. alterniflora* patches on Donghai Island, Zhanjiang. five remote sensing classification methods including RF, SVM, MLC, Minimum Distance Classification (MDC), and Mahalanobis Distance Classification (MaDC) are combined with spectral bands, spectral indices, and texture features for use, 1) to compare the accuracy of different methods in the extraction results, 2) to compare the classification effects of different features and their combinations, 3) to observe the best classification combination by pairing the methods with the features. This research provides an important reference for future research on blue carbon ecosystems in western Guangdong and contributes to the management and control of invasive species in this region.

2 Materials and methods

2.1 Study area

Donghai Island (Figure 1) covers an area of 289 km^2 (latitude 20°55'–21°05' N; longitude 110°11'–110°33' E), making it the largest

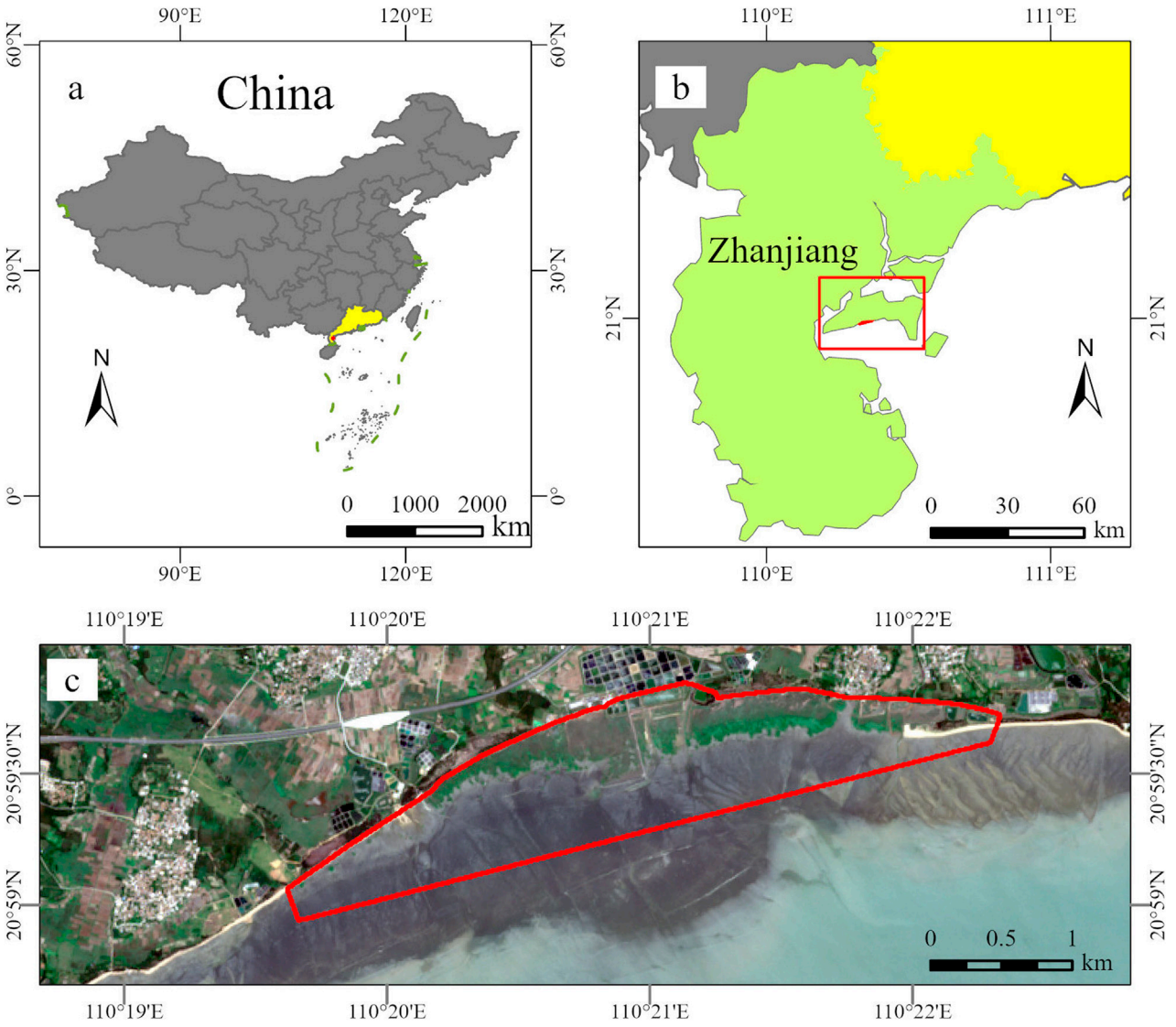

FIGURE 1
Maps of the study area: **(a)** yellow area shows Guangdong; **(b)** red box shows Donghai Island; **(c)** red line represents the target study area.

island in Guangdong Province and the fifth largest island in China. The island experiences a subtropical monsoon climate, regulated year-round by maritime influences, with an average annual temperature range of 22.7°C–23.5°C and annual precipitation of 1,395.5–1,723.1 mm. *S. alterniflora* grows in mangroves near Beishan Harbor and as abundant independent patches within a large number of tidal flats, which together form an area approximately 4.4 km long, accounting for the largest expanse of *S. alterniflora* in Zhanjiang, China.

2.2 Datasets

2.2.1 Data sources and processing

Remote sensing images were selected for the study area during periods with no cloud cover or tidal inundation. After careful screening, a Level 2A image was obtained on 11 July 2023. This image was processed using the Sen2Cor v2.11 plugin and resampled to 10-m resolution. Radiometric correction and clipping were performed to extract the target area using ENVI 5.6 software. Spectral bands B1 and B10 were removed, whereas the remaining bands were retained to calculate vegetation indices and texture features; spectral band information is provided in Table 1. This approach ensured an accurate assessment of vegetation characteristics and facilitated the analysis of *S. alterniflora* distribution within the target region.

2.2.2 Construction of SIs and texture features

In this study, we selected four vegetation indices, NDVI, EVI, red-edge NDVI, and green NDVI, along with two additional indices, the modified normalized difference water index and mSAVI, to differentiate between water bodies and intertidal zones. In addition, we employed the gray-level co-occurrence matrix (GLCM) to extract second-order texture features, such as homogeneity, contrast,

TABLE 1 Spectral band information of Sentinel-2 data.

Band number	Central wavelength (nm)	Bandwidth (nm)	Spatial resolution (m)
B1	443.9	27	60
B2	496.6	98	10
B3	560.0	45	10
B4	664.3	38	10
B5	703.9	19	20
B6	740.2	18	20
B7	782.5	28	20
B8	835.1	145	10
B8A	864.8	33	20
B9	945.0	26	60
B10	1,373.5	75	60
B11	1,613.7	143	20
B12	2,202.3	242	20

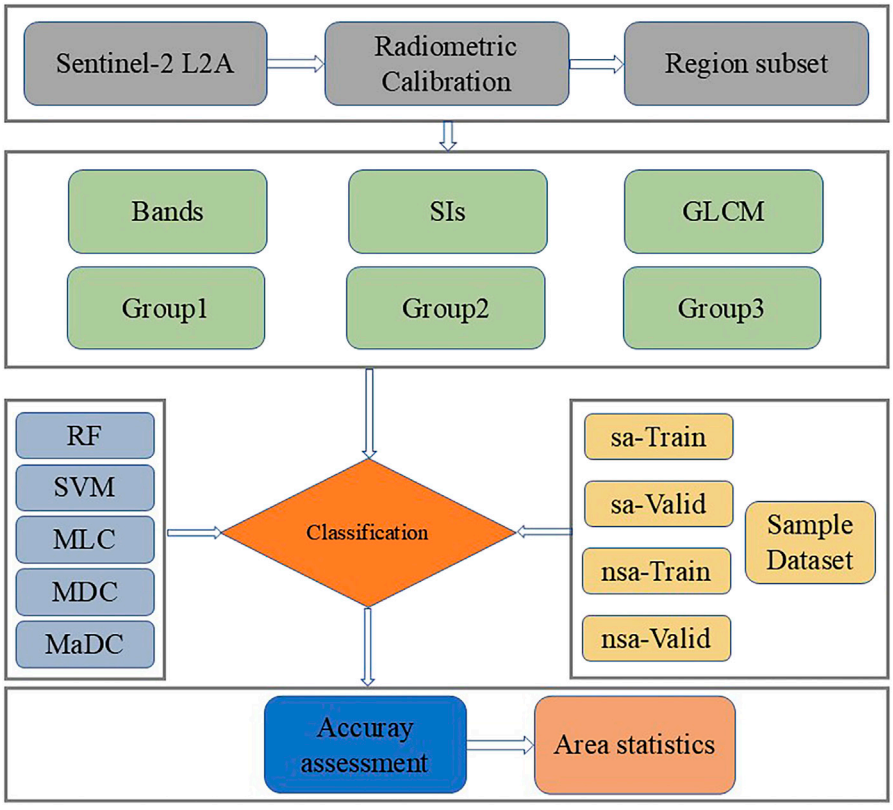

FIGURE 2
Flowchart of the classification process employed in this study.

dissimilarity, entropy, angular second moment, and correlation. First-order statistics like mean and variance were also included in the data set.

Visual interpretation of land-cover types was conducted using two primary data sources as references. The first source comprises previous literature (Xin et al., 2018; Huang et al., 2021) and the

second included very-high-spatial-resolution imagery obtained from Maxar and Google Earth. Based on these reference data, 912 sample points were established and subsequently divided into training and validation sets at a 7:3 ratio. Among the sample points, 409 pixels represented *S. alterniflora* and 503 pixels were "non-*S. alterniflora*"; these included tidal flats, mangroves, and water. This detailed sampling approach ensures robust classification and validation of land-cover types. As shown in Figure 2, the features were divided into six groups: spectral bands alone; SIs alone; GLCM alone; bands + SIs (Group 1); bands + GLCM (Group 2); and bands + SIs + GLCM (Group 3). The training sets included the *S. alterniflora* training set (sa-Train) and non-*S. alterniflora* training set (nsa-Train), and the validation sets included the *S. alterniflora* verification set (sa-Valid) and non-*S. alterniflora* verification set (nsa-Valid).

2.3 Separability calculation and classification methods

The Jeffries–Matusita (JM) distance is an important metric for assessing the spectral separability between two land-cover classes within a region of interest (Bruzzone et al., 1995). The JM distance, calculated based on the differences between the mean vectors and covariance matrices of the two classes, ranges from zero to two, where values closer to two indicate better separability in the feature space, with classes easier to distinguish using a classifier, and values closer to zero indicating that classes are increasingly difficult to differentiate (Jeffreys, 1997). Generally, JM > 1.9 indicates very good separability, whereas JM < 1 may warrant caution when merging the two samples into a single class. For classes that follow a normal distribution, the JM distance can be calculated based on Formulas 1, 2:

$$JM_{ij} = \sqrt{2^{*}\left(1 - e^{-B_{ij}}\right)} \tag{1}$$

$$B = \frac{1}{8}\left(m_i - m_j\right)^{T}\left\{\frac{C_i + C_j}{2}\right\}^{-1}\left(m_i - m_j\right) + \frac{1}{2}ln\left\{\frac{\left|\frac{(C_i+C_j)}{2}\right|}{\left|\left(C_i{}^{*}C_j\right)^{1/2}\right|}\right\} \tag{2}$$

where i and j represent the different land-cover types; m_i and m_j denote the mean values; and C_i and C_j denote the covariance matrices of the classes.

After meeting the separation requirements, the features of different groups were input into the RF, SVM, MLC, MaDC, and MDC models, and the accuracy of the classification results was evaluated using the verification set. In addition, sa and nsa area data classified using various methods were counted. A flowchart of the classification process is shown in Figure 2.

2.4 Accuracy validation

A confusion matrix was used to evaluate the performance of the classification models; this matrix displays the relationships between the actual classes and the classes predicted by the model. Various metrics were then calculated from the confusion matrix, including the overall accuracy (OA), producer accuracy, and user accuracy. The kappa coefficient is a statistical measure used to assess the level of agreement between groups and classifications; a kappa value closer to one indicates high consistency and accuracy, whereas a value closer to zero indicates low accuracy and poor agreement. The kappa coefficient was calculated based on Formula 3:

$$\text{Kappa} = \frac{N\sum_{i=1}^{n} m_{i,i} - \sum_{i=1}^{n}\left(G_i C_i\right)}{N^2 - \sum_{i=1}^{n}\left(G_i C_i\right)} \tag{3}$$

where n represents the total number of land-cover classes; N denotes the total number of pixels in the dataset; $m_{i,i}$ refers to the number of pixels in the i-th row and i-th column of the confusion matrix, indicating the number of correctly classified pixels for class i; G_i is the total number of predicted samples in the classification results for class i; and C_i is the total number of actual samples in the ground truth for class i.

3 Results

3.1 Spectral characteristics of the data

The original spectral profiles of different land-cover classes, including *S. alterniflora*, mangrove intertidal zones, water bodies, and mud, are shown in Figure 3. *S. alterniflora* showed minimal distinction from water bodies in the visible bands, whereas significant differences (>500 nm) were evident in the red-edge, near-infrared, B9, B11, and B2 bands. The reflectance values of *S. alterniflora* and intertidal zones were comparable in the visible bands, showing no significant differences in the B5 and B12 bands, whereas the differences in all other bands were >800 nm. Spectral differences between *S. alterniflora* and mangroves were similar to those between *S. alterniflora* and wetlands, primarily occurring in the B6–B9 and B11 bands. In summary, the bands that differentiate *S. alterniflora* from the other land-cover types primarily fell within the non-visible bands. Figure 4 shows that the trend of the sa dataset aligned with the spectral curves, whereas the nsa dataset showed minimal variation with increasing wavelength. The spectral bands exhibiting differences between sa and nsa datasets were B6–B9 and B11, which is similar to the spectral differences between *S. alterniflora* and mangroves. Regarding the SIs, the mean value for the nsa dataset ranged from 0.01 to 0.10, whereas that for the sa dataset ranged from 0.21 to 0.50 (Figure 5). Significant SI differences were observed between the two datasets, which is beneficial for classification.

3.2 Dataset separability

The differences in spectral bands among datasets yielded JM distance values of 1.931 and 1.900 for training and validation subsets, respectively, indicating good separability (Table 2). The separability values were lowest for the SI datasets, at 1.897 and 1.893 for training and validation sets, respectively, whereas the GLCM datasets exhibited exceptionally high separability, with

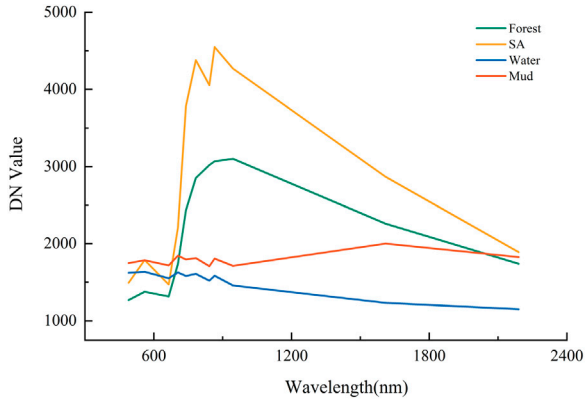

FIGURE 3
Spectral reflectance curves of different land-cover types in the study area.

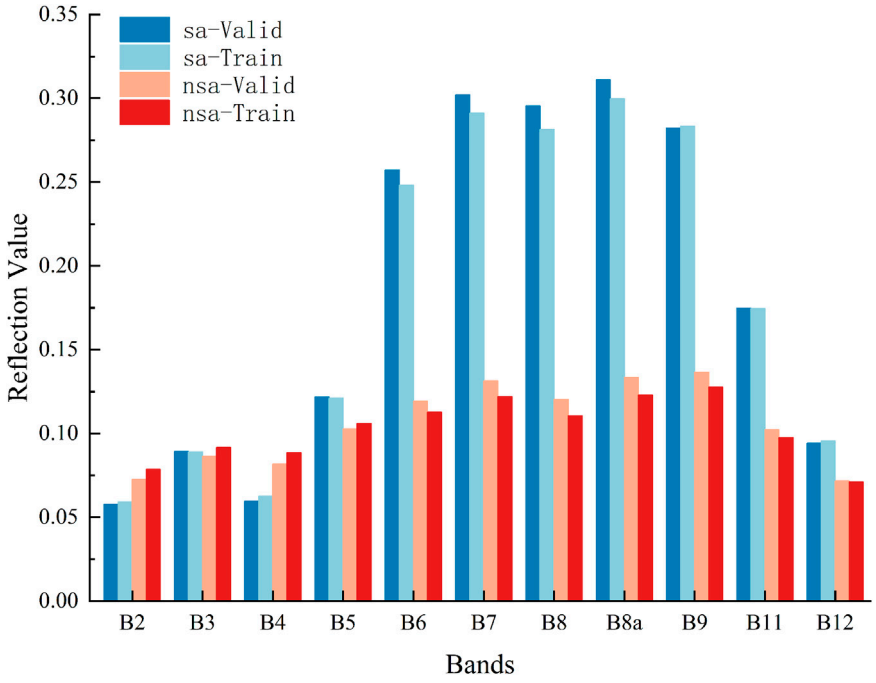

FIGURE 4
Differences in spectral bands between training and validation datasets.

both subsets exhibiting JM distances of 2.000, making them well-suited for classification tasks. As for the different feature combinations, combining spectral bands with the other two feature categories significantly enhanced separability, with Group 1 training and validation sets showing separation values of 1.997 and 1.998, respectively, and Group 2 achieving values of 2.000 for both subsets. Thus, a combination of different features is beneficial for enhancing the classification distance and facilitating the classification process. It should be noted that the combination of features in Group 3 could not be calculated using the JM distance because of substantial differences in the numerical range.

3.3 Classification accuracy

The classification results of the different algorithm–feature combinations are shown in Supplementary Figures S1–S30. The mean kappa coefficients for the five classification methods (RF, SVM, MLC, MDC, and MaDC) were 0.87, 0.83, 0.88, 0.60, and 0.82, respectively (Figure 6). The standard deviation of the RF classification method was 0.021. As the number of features increased, the kappa coefficient and OA of RF increased by 0.05% and 2.52%, respectively indicating relatively stable performance across different features, with an OA greater than 90% (Figure 7b). The MLC method achieved the best performance

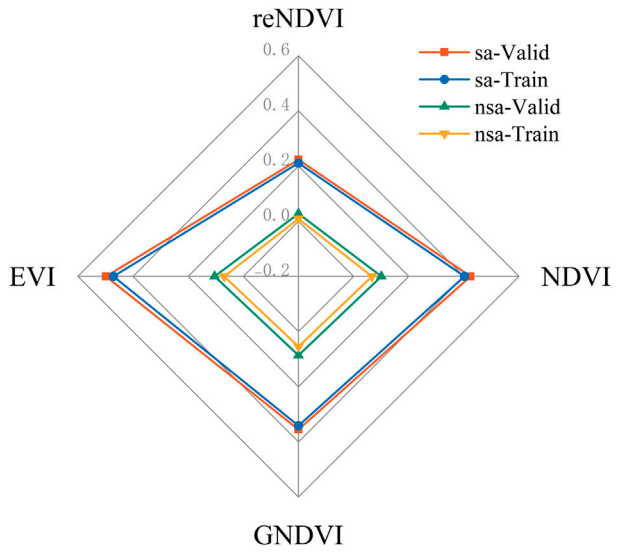

FIGURE 5
Differences in spectral indices between training and validation datasets.

TABLE 2 Jeffries–Matusita distances for different feature combinations.

Data set	GLCM	Group 2	Group 1	Bands	SIs
Training set	2.000	2.000	1.997	1.931	1.897
Validation set	2.000	2.000	1.998	1.900	1.893

with spectral features, achieving a kappa coefficient of 0.9061 and OA of 95.32%, but showed the worst performance when combined with SIs, with a kappa coefficient of 0.82 and OA of 91.01% (Figure 7a). Other features also performed well in MLC classification. For the feature combinations, classification performance improved slightly when more features were included. In SVM classification, the groups that included GLCM features exhibited better classification performance, with an OA of 93.53% (Figure 7c). The MDC classification method showed the poorest overall performance, with kappa coefficients and OA values less than 0.80% and 90% for all feature classifications, respectively (Figure 7d). MDC classification using GLCM features showed the worst combined performance, with a kappa coefficient of only 0.13, whereas the best performing feature was SIs, with a kappa coefficient of 0.77. Similar to SVM, the MaDC method achieved high classification accuracy for groups that included GLCM features, with OA values for GLCM and Group 3 features of 93.53% and 93.88%, respectively (Figure 7e).

3.4 Differences in the extracted area of *S. alterniflora*

The average area of *S. alterniflora* extracted by the RF, SVM, MLC, and MaDC methods were 75.66, 76.68, 77.65, and 82.73 ha, respectively (Table 3). After removing the outliers from GLCM features, the average area extracted by the MDC method was 81.64 ha. The area of *S. alterniflora* on Donghai Island extracted through visual interpretation was 68.69 ha. RF exhibited relatively small fluctuations in the extracted area with different feature combinations, showing a maximum difference of 2.43 ha. Although the area extracted by MLC combined with band and Group 3 features was closest to that obtained from visual interpretation, MLC exhibited relatively large fluctuations with different feature combinations, showing a maximum difference of 12.63 ha.

4 Discussion

4.1 Spectral and texture differentiation of *S. alterniflora*

As well as occupying coastal zones, *S. alterniflora* commonly coexists with salt marsh plants or mangroves. Therefore, image extraction using only spectral or phenological features alone often yields suboptimal results. Here, we combined spectral and phenological features to enhance identification accuracy and obtain more reliable target samples. The key spectral bands differentiating *S. alterniflora* from the other three land-cover types were found in the non-visible bands. Green vegetation exhibits rapid changes in the red-edge band, with healthy plants displaying the red-edge phenomenon (Horler et al., 1983). July is a rapid growth period characterized by high chlorophyll contents that may even exceed those of mangroves. This resulted in a red-shift phenomenon in *S. alterniflora*, facilitating its differentiation from mangroves in terms of NDVI and red-edge NDVI values. During low tide, some moisture remains in intertidal zones, which results in a similar overall spectral curve to water bodies, with spectral differences predominantly limited to the short-wave infrared range. *S. alterniflora* vegetation exhibits strong reflectance in the infrared band, whereas tidal flats and water bodies demonstrate higher absorption rates, which helps distinguish between tidal flats and water bodies.

In the sample dataset, the spectral bands of *sa* and nsa datasets differed primarily in the near-infrared and shortwave-infrared bands, which is consistent with the spectral differences between terrestrial objects. The vegetation index features all utilize calculations based on the near-infrared band, and differences in the spectral indices are already present; conversely, differences in the texture features derived from the GLCM increased as the dimensionality increased. The differences among the three types of features indicated that a greater difference in the mean vector values during JM distance calculation led to higher sample separability, ensuring that the samples met the classification requirements. Thus, increasing the number of classification features used in supervised classification can improve classification accuracy to a certain extent, except for unsuitable classification methods.

4.2 Optimal classification methods for *S. alterniflora* extraction

Among the five supervised classification methods, RF demonstrated good adaptability to high-dimensional data.

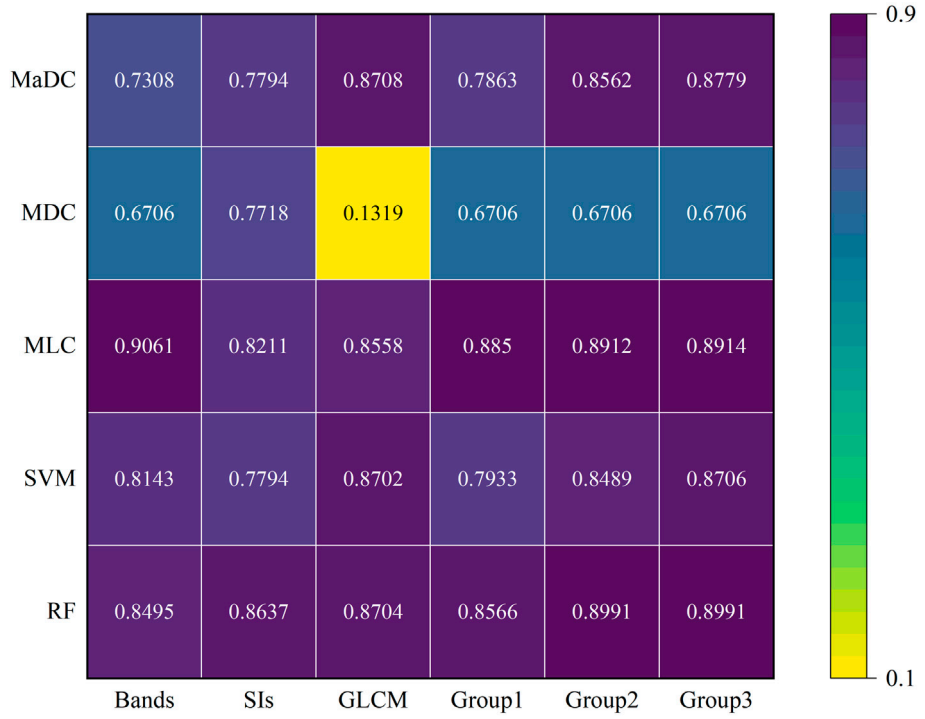

FIGURE 6
Kappa coefficients of different classification algorithm–feature combinations.

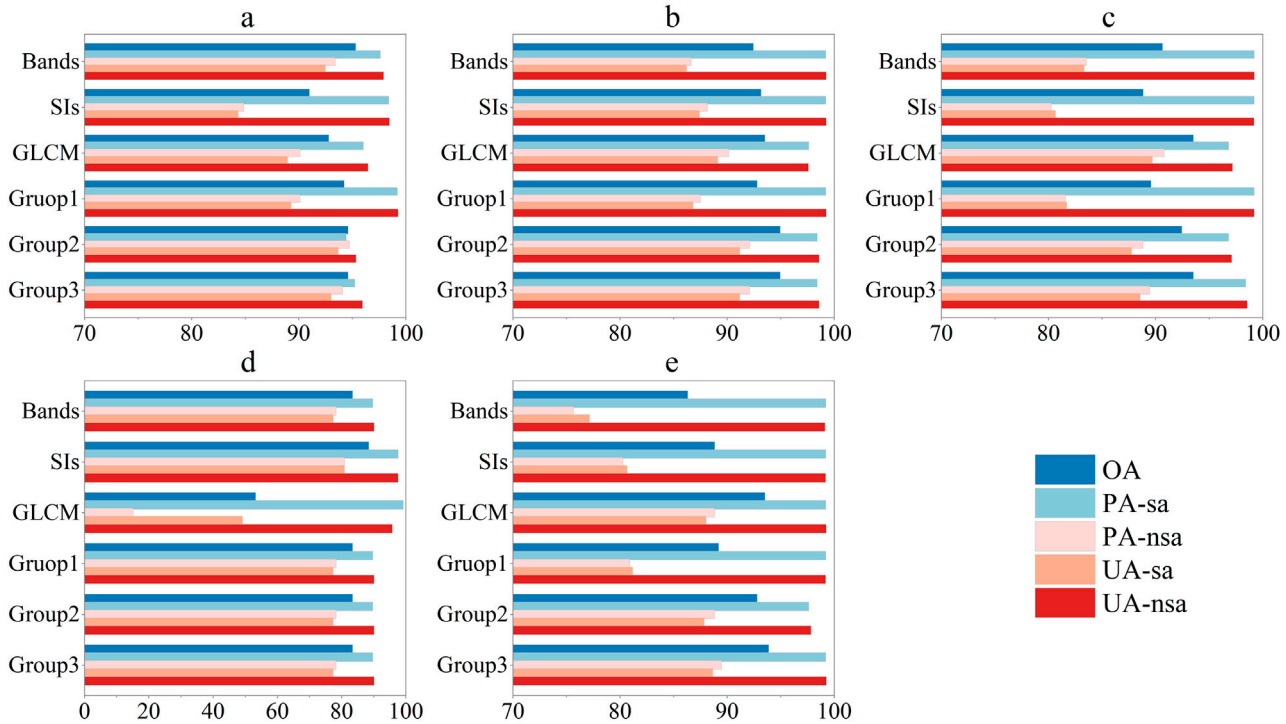

FIGURE 7
Overall accuracy, producer accuracy, and user accuracy for different features and classification methods: **(a)** maximum likelihood classification, **(b)** random forest, **(c)** support vector machine, **(d)** minimum distance classification, and **(e)** Mahalanobis distance classification.

TABLE 3 Total area of *S. alterniflora* and non-*S. alterniflora* extracted by the different algorithm–feature combinations.

Feature	Non-*S. alterniflora* area (ha)					*S. alterniflora* area (ha)				
	RF	SVM	MLC	MDC	MaDC	RF	SVM	MLC	MDC	MaDC
Bands	239.28	239.64	242.34	233.07	230.15	75.57	75.21	72.51	81.78	84.70
SIs	237.66	231.74	236.92	233.76	229.33	77.19	83.11	77.93	81.09	85.52
GLCM	239.18	240.21	229.71	51.55	237.93	75.67	74.64	85.14	263.30	76.92
Group 1	239.42	237.57	239.76	233.07	230.35	75.43	77.28	75.09	81.78	84.50
Group 2	240.09	240.21	233.39	233.07	232.22	74.76	74.64	81.46	81.78	82.63
Group 3	239.54	239.63	241.08	233.07	232.73	75.31	75.22	73.77	81.78	82.12
Average	239.20	238.17	237.20	202.93	232.12	75.66	76.68	77.65	111.92	82.73

Typically, as the feature dimensions increase, RF exhibits higher accuracy than other methods (Ye et al., 2013). For example, Yan et al. (2021) used an object-based RF algorithm to quantify the expansion and decline of *S. alterniflora* in the Dafeng River Elk Protection Area from 1993 to 2020, and achieved an OA of greater than 90%. Moreover, Tian et al. (2020) employed RF to calculate the area and expansion rate of *S. alterniflora* in the Zhangjiang Estuary from 2016 to 2018, and achieved a kappa coefficient greater than 0.89. In our study, RF classification also achieved kappa coefficients greater than 0.84 and OAs greater than 92%, showing stable results across all six groups of features.

The MLC method requires land-cover features to exhibit differences and conform to a certain probability distribution. Zhou et al. (2017) combined Spot six multispectral imagery and UAV data using MLC and NDVI to estimate the coverage of *S. alterniflora* in Sansha Bay, and achieved an RMSE of 0.117, indicating good accuracy. Hladik et al. (2013) used multisensor data, DEM, MLC, and decision tree methods to extract different ecological types of *S. alterniflora* in and around the Duplin River, achieving an OA of 90% and a kappa coefficient of 0.88. Similarly, in this study, the kappa coefficients for MLC classification ranged from 0.82 to 0.91, with OAs exceeding 91%, indicating good classification performance. The band values of the samples varied with the land-cover type, resembling a probability distribution, whereas the SIs and GLCM showed no clear probability distribution, leading to lower classification accuracy.

Compared with machine learning and statistical models, machine learning achieves the best accuracy by iteratively calculating classified data; while the classification of statistical models is based on distribution assumptions, and the rationality of the assumptions affects the accuracy of classification. In reasonable samples, RF and SVM achieve relatively high accuracy through self-iterative learning; among the three statistical models, since the methods and assumptions have different requirements, MLC and MaDC show better classification effects through covariance, while MDC only calculates the distance between category centers, and the possibility of misclassification increases as the sample points become relatively close. The five methods employed in this study showed variable adaptability to the six groups of features, resulting in significant differences in accuracy. At the methodological level, when the data dimensionality was low, RF and MLC demonstrated higher classification accuracy. As the data dimensionality increased, RF exhibited the best adaptability to high-dimensional data and achieved better classification results.

4.3 Implications for S. alterniflora management

According to previous studies, *S. alterniflora* was introduced to the eastern coastal areas of Zhanjiang in 2006 (Xin et al., 2018) but is currently distributed in multiple areas, including Gaoqiao Town in Lianjiang City, Caotan Town in Suixi County, Nansan Island in Potou District, the coastal areas of Leizhou City, Jinhe Island in Xuwen County, and Donghai Island. The area of *S. alterniflora* along the eastern coastline was 79.04 ha in 2016, which rapidly increased to 154.42 ha in 2018, with the area on Donghai Island reaching 65.34 ha in 2018 (Huang et al., 2021). According to our results, compared to the extent of *S. alterniflora* obtained by visual interpretation (68.69 ha), the area of *S. alterniflora* on Donghai Island increased by 3.35 ha over a 5-year period, indicating a growth rate of 5.13%. The *S. alterniflora* distribution in Zhanjiang Bay is primarily divided into an intertidal zone south of Donghai Island and a northern intertidal zone of Nansan Island. Influenced by factors such as tides, shorebirds, and typhoons, seeds or rhizomes can spread to suitable intertidal zones (Li et al., 2023; Zhang et al., 2023). Because of its broad tolerance to flooding and salinity (Liu et al., 2023), *S. alterniflora* initially occupies a favorable habitat in light sandy areas, then continuously reproduces and expands its population to compete for the ecological niches of other species, thus completing the invasion pattern of introduction–population establishment–reproductive stagnation–expansion. Therefore, we speculate that the relatively sparse mangroves and large area of exposed intertidal zone in Beishan Port, combined with the aforementioned conditions, enabled the expansion of *S. alterniflora* to the maximum extent in the entire western Guangdong region.

Mangroves typically comprise trees or shrubs that grow relatively slowly during their expansion into light sandy areas, with the gaps often occupied by *S. alterniflora* (Liu et al., 2023). This makes it difficult for mangrove plants to establish population dominance, leading to a reduction in growth space. Zhanjiang had the largest mangrove protection area and is greatly affected by *S. alterniflora* invasion. To protect the ecological integrity of the

mangrove ecosystem, the government has implemented measures such as cutting, filling, and plastic sheeting to curb the growth of *S. alterniflora*, with some success (Leizhou Municipal Government, 2021; Zhanjiang Daily Network Dissemination Cente, 2023; Forest Administration of Guangdong Province, 2024). However, localized control efforts only achieve short-term effects against the widespread distribution of *S. alterniflora*. Over time, *S. alterniflora* may become reestablished in these regions or even migrate from other regions. In terms of management, simultaneous clearing of the entire region is required to eliminate as many patches as possible, along with enhanced monitoring across the city to prevent overlooked patches from forming populations. Additionally, the introduction of native plants into cleared intertidal zones should be employed to restrict potential *S. alterniflora* habitats.

4.4 Limitation of the classification methods

The uncertainty of the data, the lack of actual survey data that matches the date of remote sensing images, and the certain deviations in classification due to this. In terms of the model, the classification precision of some models is too low to meet the classification requirements, and the models lack broader validation. In terms of parameters, the automatic calculation parameters of ENVI are used, and the correlation between parameter adjustment and classification accuracy has not been studied in detail.

5 Conclusion

In this study, we explored the accuracy of *S. alterniflora* classification by integrating five common supervised classification methods with six groups of features. This approach encompassed both common machine learning and traditional classification methods, as well as the main classification features, providing an important reference for *S. alterniflora* monitoring in mangrove areas. The main findings were as follows. 1) RF showed better classification performance across different features, particularly for high-dimensional data, demonstrating high classification stability and applicability to various classification scenarios. 2) For spectral band data, the MLC classification method yielded the best results. 3) During classification, acquiring spectral indices and textural features based on spectral band information can enhance the classification accuracy. 4) *S. alterniflora* on Donghai Island requires systematic management, and the possibility of re-invasion after cleaning should be reduced by cleaning, monitoring, and introducing native plants. These findings have important implications for the monitoring and management of invasive species. Some limitations regarding the input data, modeling and parameters can be further investigated.

Data availability statement

The original contributions presented in the study are included in the article/Supplementary Material, further inquiries can be directed to the corresponding authors.

Author contributions

QC: Validation, Data curation, Visualization, Methodology, Conceptualization, Writing – review and editing, Writing – original draft, Software, Formal Analysis, Project administration. CS: Supervision, Writing – review and editing. HD: Supervision, Writing – review and editing. DT: Writing – review and editing, Funding acquisition, Supervision.

Funding

The author(s) declare that financial support was received for the research and/or publication of this article. Supported by the Guangdong special support plan for Key Talents Team Program (No. 2019BT02H594), the PI Project of Southern Marine Science and Engineering Guangdong Laboratory (Guangzhou) (No.GML2021GD0810), the Dragon 6 Programme (No.PP95531) and Guangdong Province Special Project on Pollution Prevention and Protection and Eco-environmental Protection.

Acknowledgments

We thank the European Space Agency for the provision of data necessary for this study.

Conflict of interest

The authors declare that the research was conducted in the absence of any commercial or financial relationships that could be construed as a potential conflict of interest.

Generative AI statement

The author(s) declare that no Generative AI was used in the creation of this manuscript.

Publisher's note

Supplementary material

The Supplementary Material for this article can be found online at: https://www.frontiersin.org/articles/10.3389/frsen.2025.1606549/full#supplementary-material

References

Ahmed, N., Cheung, W. W. L., Thompson, S., and Glaser, M. (2017). Solutions to blue carbon emissions: shrimp cultivation, mangrove deforestation and climate change in coastal Bangladesh. *Mar. Policy* 82, 68–75. doi:10.1016/j.marpol.2017.05.007

Ai, J., Gao, W., Gao, Z., Shi, R., and Zhang, C. (2017). Phenology-based Spartina alterniflora mapping in coastal wetland of the Yangtze Estuary using time series of GaoFen satellite no. 1 wide field of view imagery. *J. Appl. Remote Sens.* 11 (2), 026020. doi:10.1117/1.JRS.11.026020

Ainouche, M. L., Baumel, A., Salmon, A., and Yannic, G. (2004). Hybridization, polyploidy and speciation in Spartina (poaceae). *New Phytol.* 161 (1), 165–172. doi:10.1046/j.1469-8137.2003.00926.x

Aryal, A., Kim, K. Y., and Lakshmi, V. (2025). Understanding flood dynamics in the indus river basin: lessons from the 2022 Pakistan deluge. *J. Hydrology Regional Stud.* 59, 102362. doi:10.1016/j.ejrh.2025.102362

Banerjee, A. K., Liang, X., Harms, N. E., Tan, F., Lin, Y., Feng, H., et al. (2022). Spatio-temporal pattern of cross-continental invasion: evidence of climatic niche shift and predicted range expansion provide management insights for smooth cordgrass. *Ecol. Indic.* 140, 109052. doi:10.1016/j.ecolind.2022.109052

Bruzzone, L., Roli, F., and Serpico, S. B. (1995). An extension of the Jeffreys-Matusita distance to multiclass cases for feature selection. *IEEE Trans. Geoscience Remote Sens.* 33 (6), 1318–1321. doi:10.1109/36.477187

Candotti, A., Giglio, M. D., Dubbini, M., and Tomelleri, E. (2022). A sentinel-2 based multi-temporal monitoring framework for wind and bark beetle detection and damage mapping. *Remote Sens.* 14 (23), 6105. doi:10.3390/rs14236105

Chu, D., Liu, L., Wang, Z., Nie, Y., and Zhang, Y. (2024). Snow avalanche hazards and avalanche-prone area mappingin tibet. *Geosciences* 14 (12), 353. doi:10.3390/geosciences14120353

Chung, C. H. (2006). Forty years of ecological engineering with Spartina plantations in China. *Ecol. Eng.* 27 (1), 49–57. doi:10.1016/j.ecoleng.2005.09.012

Dawson, W., Moser, D., Van Kleunen, M., Kreft, H., Pergl, J., Pyšek, P., et al. (2017). Global hotspots and correlates of alien species richness across taxonomic groups. *Nat. Ecol. and Evol.* 1 (7), 0186–0187. doi:10.1038/s41559-017-0186

Du, Y., Zhang, Y., Ling, F., Wang, Q., Li, W., and Li, X. (2016). Water bodies' mapping from sentinel-2 imagery with modified normalized difference water index at 10-m spatial resolution produced by sharpening the SWIR band. *Remote Sens.* 8 (4), 354. doi:10.3390/rs8040354

Forest Administration of Guangdong Province (2024). The Provincial Forestry Bureau held an exchange activity on Spartina alterniflora prevention and control [OL]. Available online at: https://lyj.gd.gov.cn/news/forestry/content/post_4494321.html.

Fu, B., He, X., Yao, H., Liang, Y., Deng, T., He, H., et al. (2022). Comparison of RFE-DL and stacking ensemble learning algorithms for classifying mangrove species on UAV multispectral images. *Int. J. Appl. Earth Observation Geoinformation* 112, 102890. doi:10.1016/j.jag.2022.102890

Hanif, F., Kanae, S., Farooq, R., Iqbal, M. R., and Petroselli, A. (2023). Impact of satellite-derived land cover resolution using machine learning and hydrological simulations. *Remote Sens.* 15 (22), 5338. doi:10.3390/rs15225338

Hartley, R. J. L., Leonardo, E. M., Massam, P., Watt, M. S., Estarija, H. J., Wright, L., et al. (2020). An assessment of high-density UAV point clouds for the measurement of young Forestry trials. *Remote Sens.* 12 (24), 4039. doi:10.3390/rs12244039

Hladik, C., Schalles, J., and Alber, M. (2013). Salt marsh elevation and habitat mapping using hyperspectral and LIDAR data. *REMOTE Sens. Environ.* 139, 318–330. doi:10.1016/j.rse.2013.08.003

Horler, D. N. H., Dockray, M., and Barber, J. (1983). The red edge of plant leaf reflectance. *Int. J. Remote Sens.* 4 (2), 273–288. doi:10.1080/01431168308948546

Hosseini, M. M., Zoej, M. J. V., and Taheri, A. (2024). Cropping intensity mapping in Sentinel-2 and Landsat-8/9 remote sensing data using temporal transfer. *Geocarto Int.* 39 (1), 2387786. doi:10.1080/10106049.2024.2387786

Huang, H., Li, Z., Jin, W., Tan, Q., and Zhao, S. (2021). Remote sensing monitoring and analysis of invasion plant Spartina alterniflora in Leizhou peninsula. *For. Enviromental Sci.* 37 (3), 22–27.

Jeffreys, H. (1997). An invariant form for the prior probability in estimation problems. *Proc. R. Soc. Lond. Ser. A. Math. Phys. Sci.* 186 (1007), 453–461. doi:10.1098/rspa.1946.0056

Leizhou Municipal Government (2021). The Handbook of Mangrove Ecological Restoration was published and the cases of Leizhou mangrove forest area were selected [OL]. Available online at: http://www.leizhou.gov.cn/xwdt/lzyw/content/post_1530143.html.

Li, C., Chen, J., Liao, X., Ramus, A. P., Angelini, C., Liu, L., et al. (2023). Shorebirds-driven trophic cascade helps restore coastal wetland multifunctionality. *Nat. Commun.* 14 (1), 8076. doi:10.1038/s41467-023-43951-3

Li, M., Shamshiri, R. R., Weltzien, C., and Schirrmann, M. (2022a). Crop monitoring using sentinel-2 and UAV multispectral imagery: a comparison case study in northeastern Germany. *Remote Sens.* 14 (17), 4426. doi:10.3390/rs14174426

Li, Y., Fu, B., Sun, X., Fan, D., Wang, Y., He, H., et al. (2022b). Comparison of different transfer learning methods for classification of mangrove communities using MCCUNet and UAV multispectral images. *Remote Sens.* 14 (21), 5533. doi:10.3390/rs14215533

Liu, M., Mao, D., Wang, Z., Li, L., Man, W., Jia, M., et al. (2018). Rapid invasion of Spartina alterniflora in the coastal zone of mainland China: new observations from Landsat OLI images. *Remote Sens.* 10 (12), 1933. doi:10.3390/rs10121933

Liu, Q., Li, Y., and Wang, P. (2023). Research progresses in invasion ecology of exoticspecies Spartina alterniflor. *Trans. Oceanol. Limnol.* 45 (3), 155–163. doi:10.13984/j.cnki.cn37-1141.2023.03.021

Min, Y., Cui, L., Li, J., Han, Y., Zhuo, Z., Yin, X., et al. (2023). Detection of large-scale Spartina alterniflora removal in coastal wetlands based on Sentinel-2 and Landsat 8 imagery on Google Earth Engine. *Int. J. Appl. Earth Observation Geoinformation* 125, 103567. doi:10.1016/j.jag.2023.103567

Morris, J. T., Porter, D., Neet, M., Noble, P. A., Schmidt, L., Lapine, L. A., et al. (2005). Integrating LIDAR elevation data, multi-spectral imagery and neural network modelling for marsh characterization. *Int. J. Remote Sens.* 26 (23), 5221–5234. doi:10.1080/01431160500219018

National Forestry and Grassland Administration (2025). Special action plan for Spartina alterniflora control (2022-2025). Available online at: https://www.gov.cn/xinwen/2023-03/16/content_5747029.htm.

O'Donnell, J. P. R., and Schalles, J. F. (2016). Examination of abiotic drivers and their influence on Spartina alterniflora biomass over a twenty-eight year period using Landsat 5 TM satellite imagery of the Central Georgia Coast. *REMOTE Sens.* 8 (6), 477. doi:10.3390/rs8060477

Ondieki, J. O., Mito, C., and Kaniu, M. (2022). Feasibility of mapping radioactive minerals in high background radiation areas using remote sensing techniques. *Int. J. Appl. Earth Observation Geoinformation* 107, 102700. doi:10.1016/j.jag.2022.102700

Saim, A. A., and Aly, M. (2025). Enhancing tree species mapping in Arkansas' forests through machine learning and satellite data fusion: a Google Earth engine–based approach. *J. Geovisualization Spatial Analysis* 9 (1), 20. doi:10.1007/s41651-025-00220-9

Sharma, S., Sedona, R., Riedel, M., Cavallaro, G., and Paris, C. (2024). Sen4Map: advancing mapping with sentinel-2 by providing detailed semantic descriptions and customizable land-use and land-cover data. *IEEE J. Sel. Top. Appl. EARTH OBSERVATIONS REMOTE Sens.* 17, 13893–13907. doi:10.1109/JSTARS.2024.3435081

Sidik, F., Lawrence, A., Wagey, T., Zamzani, F., and Lovelock, C. E. (2023). Blue carbon: a new paradigm of mangrove conservation and management in Indonesia. *Mar. Policy* 147, 105388. doi:10.1016/j.marpol.2022.105388

Tian, Y., Jia, M., Wang, Z., Mao, D., Du, B., and Wang, C. (2020). Monitoring invasion process of Spartina alterniflora by seasonal sentinel-2 imagery and an object-based random forest classification. *Remote Sens.* 12 (9), 1383. doi:10.3390/rs12091383

Xin, G., Weisheng, P., Yuechao, C., Wei, Z., Tao, H., Yiming, L., et al. (2018). Invasion of Spartina alterniflora and protection of mangroves in Guangdong Zhanjiang mangrove national nature reserve and adjacent coastal area. *For. Enviromental Sci.* 34 (4), 58–63.

Xu, N., Jia, D., Ding, L., and Wu, Y. (2018). Continuously tracking the annual changes of the Hengsha and changxing islands at the Yangtze River Estuary from 1987 to 2016 using Landsat imagery. *Water* 10 (2), 171. doi:10.3390/w10020171

Yan, D., Li, J., Yao, X., and Luan, Z. (2021). Quantifying the long-term expansion and dieback of Spartina alterniflora using Google Earth engine and object-based hierarchical random forest classification. *IEEE J. Sel. Top. Appl. EARTH OBSERVATIONS REMOTE Sens.* 14, 9781–9793. doi:10.1109/JSTARS.2021.3114116

Ye, Y., Wu, Q., Zhexue Huang, J., Ng, M. K., and Li, X. (2013). Stratified sampling for feature subspace selection in random forests for high dimensional data. *Pattern Recognit.* 46 (3), 769–787. doi:10.1016/j.patcog.2012.09.005

Zhang, C., Gong, Z., Qiu, H., Zhang, Y., and Zhou, D. (2021). Mapping typical salt-marsh species in the Yellow River Delta wetland supported by temporal-spatial-spectral multidimensional features. *Sci. Total Environ.* 783, 147061. doi:10.1016/j.scitotenv.2021.147061

Zhang, X., Xiao, X., Wang, X., Xu, X., Qiu, S., Pan, L., et al. (2023). Continual expansion of Spartina alterniflora in the temperate and subtropical coastal zones of China during 1985–2020. *Int. J. Appl. Earth Observation Geoinformation* 117, 103192. doi:10.1016/j.jag.2023.103192

Zhanjiang Daily Network Dissemination Cente (2023). Clean up the invasive species Spartina alterniflora [OL]. Available online at: https://www.gdzjdaily.com.cn/p/2861467.html.

Zhao, B., Yan, Y., Guo, H., He, M., and Li, B. (2009). Monitoring rapid vegetation succession in estuarine wetland using time series MODIS-based indicators: an application in the Yangtze River Delta area. *Ecol. Indic.* 9 (2), 346–356. doi:10.1016/j.ecolind.2008.05.009

Zhou, X., Zuo, Y., Zheng, K., Shao, C., Shao, S., Sun, W., et al. (2024). Monitoring the invasion of S. Alterniflora on the Yangtze River Delta, China, using time series Landsat images during 1990–2022. *Remote Sens. (Basel).* 16, 1377. doi:10.3390/rs16081377

Zhou, Z., Yang, Y., and Chen, B. (2017). Estimating the *Spartina alterniflora* fractional vegetation cover using high spatial resolution remote sensing in a coastal wetland. *Acta Ecol. Sin.* 37 (2). doi:10.5846/stxb201507271566

Zhu, C., Zhang, X., and Qi, J. (2016). Detecting and assessing Spartina invasion in coastal region of China: a case study in the Xiangshan Bay. *Acta Oceanol. Sin.* 35 (4), 35–43. doi:10.1007/s13131-016-0836-7

Zhu, W., Ren, G., Wang, J., Wang, J., Hu, Y., Lin, Z., et al. (2022). Monitoring the invasive plant Spartina alterniflora in jiangsu coastal wetland using MRCNN and long-time series Landsat data. *Remote Sens.* 14 (11), 2630. doi:10.3390/rs14112630